Polyhedron 185 (2020) 114592

Contents lists available at ScienceDirect

Polyhedron

journal homepage: www.elsevier.com/locate/poly

Fluorescent di-(2-picolyl)amine based drug-like ligands and their $Re(CO)_3$ complexes towards biological applications

Taniya Darshani [a], Nadini Thushara [a], Piyumali Weerasuriya [a], Frank R. Fronczek [b], Inoka C. Perera [c], Theshini Perera [a,*]

[a] Department of Chemistry, University of Sri Jayewardenepura, Sri Lanka
[b] Department of Chemistry, Louisiana State University, Baton Rouge, LA 70803, United States
[c] Department of Zoology and Environment Science, University of Colombo, Sri Lanka

ARTICLE INFO

Article history:
Received 30 January 2020
Revised 22 April 2020
Accepted 26 April 2020
Available online 1 May 2020

Dedicated with much admiration to Professor Luigi G. Marzilli on the occasion of his retirement.

Keywords:
Rhenium(I) tricarbonyl complexes
Di(2-picolylamine)
Naphthyl
Dansyl
Drug-like

ABSTRACT

Herein we report two new *fac*-Re(I) tricarbonyl complexes, *fac*-[$Re(CO)_3(N(SO_2)$(1-nap)dpa)]PF_6 (**C1**) and *fac*-[$Re(CO)_3(N(SO_2)$(2-nap)dpa)]PF_6 (**C2**), of two naphthalene derivatized tridentate ligands ($N(SO_2)$(1-nap)dpa (**L1**) and $N(SO_2)$(2-nap)dpa (**L2**)) and one reported Re(I) complex, *fac*-[$Re(CO)_3(N(SO_2Me_2Nnap)$dpa)]PF_6 (**C3**), of a dansyl appended di-2-picolylamine ligand ($N(SO_2Me_2Nnap)$dpa (**L3**)). The properties of the compounds were elucidated using spectrophotometric measurements (UV–Vis, FTIR and ^1H NMR). A single crystal X-ray study was carried out for the three ligands. The ^1H NMR spectra of the three complexes obtained in DMSO d_6 displayed two doublets (*exo*-CH and *endo*-CH) for the magnetically inequivalent methylene protons, compared to their uncoordinated ligands where the methylene protons show a singlet peak. The formation of the metal complexes was further supported by FTIR spectra in which the S—N stretching band for the metal complexes appears at lower wavenumbers compared to that of the corresponding free ligands. In comparison with the uncoordinated ligands, the Re(I) complexes, **C1** and **C3**, displayed a bathochromic shift while **C2** showed a hypsochromic shift in the absorption spectra in methanol. The fluorescent maxima and the fluorescence quantum yield (ΦF) of **L1** and **L2** were 338 nm (ΦF = 0.056) and 343 nm (ΦF = 0.039), respectively. Interestingly, all the compounds except **C2** showed excellent fluorescent emissions. Biologically, the compounds were investigated for their cytotoxicity *in vitro* on human lymphocytes following the Trypan blue dye exclusion method. It was observed that both Re(I) complexes as well as the ligands show low toxicity towards human lymphocytes at working concentrations below 10 mg/ml (**L1**, **L2**: 0.026 M, **L3**: 0.023 M, **C1**, **C2**, **C3**: 0.012 M). *In silico* studies revealed that the ligands are potential candidates for anti-inflammatory agents and this was further supported by molecular docking studies, in which they showed a higher affinity for Prostaglandin synthase 2. These drug-like molecules, having an affinity to bovine serum albumin, are thus potential drug leads for anti-inflammatory agents.

1. Introduction

Metal complexes are widely used in the treatment [1–3] and diagnosis [4–6] of many diseases, out of which their use in diagnosing and treating various types of cancers is paramount. An increasing number of transition metals, such as ^{99m}Tc, Re(I), Ir(III), Rh(III), and Pt(II), have been used in synthesizing metallopharmaceuticals [4,7–12], while many serve as promising cell imaging agents due to their promising biomedical properties, such as radioactivity and attractive intrinsic photo-physical properties [13]. Most importantly, "cold" rhenium complexes have many applications in fluorescence imaging [14–16] and therapeutic applications [17]; they also serve as model systems for ^{99m}Tc [18–20], which is the most widely used radionuclide in nuclear medicine. Furthermore, the $^{188/186}Re$ isotopes are beta emitters and as such are used to treat cancers [19,21]. Of note is a recent report on the development of a multifunctional silica platform as a method to utilize the ^{99m}Tc-Re pair, integrating diagnosis and therapy [22].

Even though numerous studies have been reported on metal–ligand complexes, their chemical properties and their photophysical properties, not many *in vivo* studies have been reported on their applications as bio imaging agents [5,23–27]. Rhenium(I) metal

* Corresponding author.
E-mail address: theshi@sjp.ac.lk (T. Perera).

https://doi.org/10.1016/j.poly.2020.114592
0277-5387/

complexes are generally favoured over other metals due to their kinetic inertness, long lifetime, large Stokes shift and ligand-determined-target specificity [26,28]. As the Re metal complex is kinetically inert, it avoids ligand substitution [28]. The longer lifetime and large Stokes shift [29] minimize the self-quenching effect of the compound and facilitate *in vitro* cell imaging [15,30]. A notable source of support for the above findings emerged from the observations of Leonidova and Gasser [1], as well as Fernández-Moreira [5], that Re organometallic complexes may be utilized as useful fluorophores in bio cell imaging. Lipophilicity, toxicity and localization of the fluorophore have to be considered when utilizing it as a cell imaging agent [13]. A comprehensive overview by Balasingham *et al.* reported the cellular uptake and localization of complexes with the *fac*-$Re(CO)_3$ core [31].

We were motivated by the previously reported studies on dipicolylamine (dpa) based ligands [32–35] which exhibit promising pharmacological properties. Symmetrically complexed radiopharmaceuticals derived from dipicolylamine (dpa), such as glucosamine-dpa, have been synthesized and evaluated as imaging and therapeutic agents [35]. Furthermore, the tertiary sulfonamide linkage has been shown to be viable in bio conjugation, as well as a model system for radiopharmaceuticals [6]. Just last year, we reported [32] that *fac*-$[Re(CO)_3(NSO_2Rdpa)]^+$ (where R = piperidine) may serve as a potential pharmaceutical for the therapy of human breast cancer, mainly because these types of compounds preferentially bind with sigma receptors. Herein, our focus is on naphthalene derivatives, because naphthalene derivatized compounds have been reported to possess anti-inflammatory [36–38], antibacterial [36,39,40], antifungal and anticancer properties [41], and on the group dansyl because of its desired fluorescent properties such as high fluorescence quantum yield and large Stokes shift [42].

Non-steroidal anti-inflammatory drugs play a vital role in treating many diseases by inhibiting cyclooxygenase (COX-1 and COX-2) enzymes which are responsible for the synthesis of prostaglandins. The inflammatory process is a result of the production of prostaglandins. Therefore, much effort has been made in previous studies that describe the synthesis of potential anti-inflammatory drugs [43,44]. However, to the best of our knowledge, no reports exist where the $dpaSO_2$ scaffold is being used in synthesizing anti-inflammatory agents. Thus, in this study, two ligands *N*(SO_2R)dpa (R = 1-naphthalene, 2-naphthalene) and one reported ligand *N*(SO_2R)dpa (R = 5-(dimethylamino)naphthalene) derived from di-(2-picolyl)amine, all containing a tertiary sulfonamide group [45], and their corresponding Re(I) complexes were synthesized (Fig. 1). The chemical and biological properties of the compounds were evaluated to attest their application as potential biological agents. The ligands were screened for their drug-likeness and molecular docking studies were carried out to evaluate the preferred orientation, binding site and binding affinity of the ligands to BSA (Bovine Serum Albumin). The anti-inflammatory activity of the ligands was predicted and affinity to Prostaglandin synthase 2 (COX-2) was analyzed *in silico*.

2. Experimental

2.1. Starting materials

1-naphthalenesulfonyl chloride ((1-nap)SO_2Cl), 2-naphthalenesulfonyl chloride ((2-nap)SO_2Cl), 5-(dimethylamino)naphthalene-1-sulfonyl chloride ($Me_2NnapSO_2Cl$, dansyl chloride), di-(2-picolyl) amine (*N*(H)dpa) and $Re_2(CO)_{10}$ were used as received from Sigma-Aldrich. All other chemicals were of reagent grade and used as received, unless otherwise specified. $[Re(CO)_3(H_2O)_3]OTf$ (OTf = trifluoromethanesulfonate) was prepared by a known method [46].

2.2. Methodology

TLC analysis was performed and visualized with ultraviolet light. UV–Vis absorption spectra were obtained using a GENESIS 10S UV–Vis spectrophotometer. FTIR spectra were recorded with a Thermo Scientific NICOLET iS10 spectrometer. Fluorescence spectra were obtained using a Thermo Scientific Lumina spectrophotometer. Solutions were prepared by dissolving the analyte in methanol. Spectral data were processed with Luminous software. Quantum yield measurements were taken by preparing solutions of the test samples with increasing concentrations. The absorbance

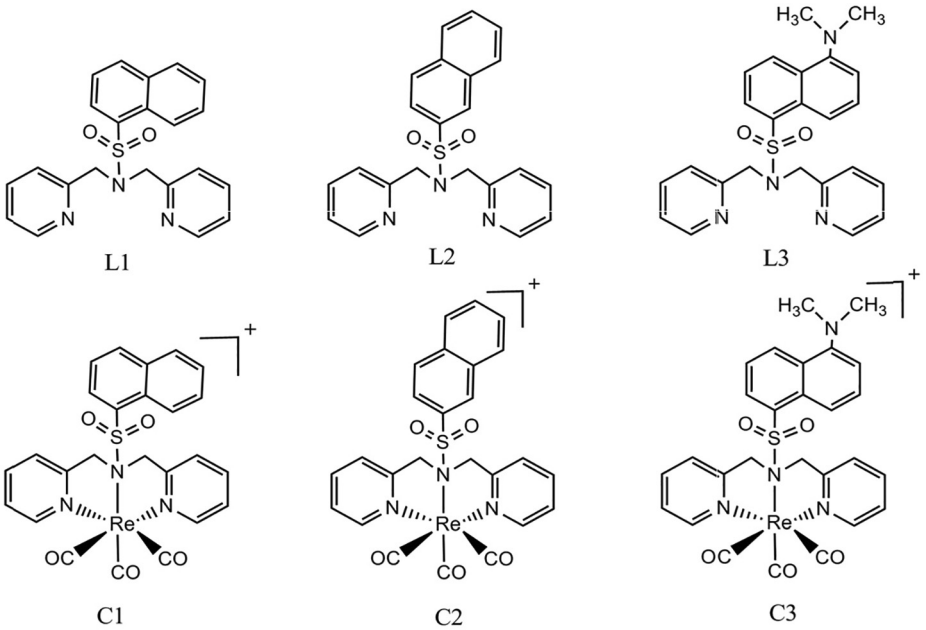

Fig. 1. Ligands and the complexes used in the study: *N*(SO_2)(1-nap)dpa (**L1**), *N*(SO_2)(2-nap)dpa (**L2**), *N*(SO_2Me_2Nnap)dpa (**L3**), *fac*-$[Re(CO)_3(N(SO_2)(1\text{-nap})dpa)]PF_6$ (**C1**), *fac*-$[Re(CO)_3(N(SO_2)(2\text{-nap})dpa)]PF_6$ (**C2**), *fac*-$[Re(CO)_3(N(SO_2Me_2Nnap)dpa)]PF_6$ (**C3**).

was recorded in methanol. The samples were excited at 280 nm and fluorescence spectra were recorded in the same solvent using a 10 mm fluorescence cuvette. The slit width was kept as 10/10 nm with scan speed of 60 nm/min. The integrated fluorescence intensity was calculated from the spectra. Tryptophan was used as a standard sample and the same steps were followed to calculate the integrated fluorescence intensity. ^{1}H NMR spectra were recorded on a Bruker 400 MHz spectrometer in DMSO d_6. Peak positions are relative to tetramethylsilane (TMS) and the data were analysed with MestReNova software. X-ray data was collected using a Bruker Kappa APEX-II diffractometer at low temperature. Cell refinement and data reduction were performed using Bruker SAINT. The SHELXS97 program was used to solve the structures and the SHELXL2014/7 program was used to refine the structures.

2.2.1. Synthesis of the [Re(CO)$_3$L]PF$_6$ complexes

The following general procedure was employed to obtain the *N*(SO_2R)dpa ligands. A solution of the sulfonyl chloride (2.5 mmol) in 12.5 ml of dioxane was added dropwise over a period of 2 h to a solution of *N*(H)dpa (0.92 ml, 5 mmol) in 50 ml of dioxane at 20 °C. The reaction mixture was stirred at room temperature for 24 h and then filtered to remove any precipitate before the dioxane was completely removed by rotary evaporation. Water (30 ml, pH ~5) was added to the resulting oil and the product was extracted into CH_2Cl_2 (2 × 25 ml), and then dried to yield an oil which was used to synthesize the [Re(CO)$_3$L]PF$_6$ complexes. A solution of the *N*(SO_2R)dpa ligand (0.1 mmol) in 2 ml of water and 3 ml of methanol was treated with aqueous [Re(CO)$_3$(H_2O)$_3$]OTf (0.1 mmol). Methanol (3 ml) was added to dissolve the precipitate formed (pH ~6). The clear reaction mixture was heated at reflux overnight (12–16 h). A slight excess of $NaPF_6$ (~20 mg) was added to the clear solution. The resulting precipitate was collected on a filter and dried.

*2.2.2. Synthesis of [Re(CO)$_3$(N(SO_2)(1-nap)dpa)]PF$_6$ (**C1**)*

Above described method with 1-naphthalenesulfonyl chloride (0.58 g, 2.5 mmol) and N(H)dpa yielded the N(SO_2)(1-nap)dpa ligand (**L1**) as a brown oil (0.75 g, 77% yield). R_f = 0.11 (dichloromethane/hexane 7:3). FTIR (cm^{-1}): 1321, 1131 (S═O); 917 (S—N). ^{1}H NMR (400 MHz, DMSO d_6) δ (ppm): 8.60 (d, *J* = 8.5 Hz, 1H), 8.32 (d, *J* = 4.1 Hz, 2H, H6/6′), 8.21 (d, *J* = 2.9 Hz, 1H), 8.19 (d, *J* = 2.0 Hz, 1H), 8.07 (d, *J* = 8.3 Hz, 1H), 7.58–7.71 (m, 3H), 7.55 (t, *J* = 7.7 Hz, 2H, H4/4′), 7.15 (t, 2H, H5/5′), 7.10 (d, *J* = 7.8 Hz, 2H, H3/3′), 4.70 (s, 4H, CH_2). Treatment of the ligand (0.039 g) with [Re(CO)$_3$(H_2O)$_3$]$^+$ (1.00 ml) as described above yielded [Re(CO)$_3$(*N*(SO_2)(1-nap)dpa)]PF$_6$ as white crystals (0.062 g, 83% yield). R_f = 0.09 (ethanol/hexane 6:4). FTIR (cm^{-1}): 2025, 1899 (C═O); 1371, 1164 (S═O); 808 (S—N). ^{1}H NMR (400 MHz, DMSO d_6) δ (ppm): 8.95 (d, *J* = 8.6 Hz, 1H), 8.90 (d, *J* = 5.1 Hz, 2H, H6/6′), 8.72 (t, 2H), 8.33 (d, *J* = 7.3 Hz, 1H), 7.98 (t, 3H, H4/4′), 7.83–7.93 (m, 2H), 7.47 (t, 2H, H5/5′), 7.37 (d, *J* = 7.9 Hz, 2H, H3/3′), 5.66 (d, *J* = 15.7 Hz, 2H, CH_2), 4.52 (d, *J* = 15.7 Hz, 2H, CH_2).

*2.2.3. Synthesis of [Re(CO)$_3$(N(SO_2)(2-nap)dpa)]PF$_6$ (**C2**)*

The above described method with 2-naphthalenesulfonyl chloride (0.57 g) and *N*(H)dpa yielded the *N*(SO_2)(2-nap)dpa ligand (**L2**) as a brown oil (0.76 g, 78% yield). R_f = 0.52 (ethanol/hexane 7:3). FTIR (cm^{-1}): 1334, 1146 (S═O); 928 (S—N). ^{1}H NMR (400 MHz, DMSO d_6) δ (ppm): 8.48 (s, 1H), 8.32 (d, *J* = 4.8 Hz, 2H, H6/6′), 8.12 (d, *J* = 7.9 Hz, 1H), 8.06 (t, 2H), 7.82 (d, *J* = 8.8 Hz, 1H), 7.66–7.73 (m, 2H), 7.63 (t, 2H, H4/4′), 7.29 (d, *J* = 7.8 Hz, 2H, H3/3′), 7.15 (t, 2H, H5/5′), 4.60 (s, 4H, CH_2). Treatment of the ligand (0.039 g) with [Re(CO)$_3$(H_2O)$_3$]$^+$ (1.00 ml) as described above yielded [Re(CO)$_3$(*N*(SO_2)(2-nap)dpa)]PF$_6$ as white crystals (0.038 g, 47% yield). R_f = 0.14 (ethanol/hexane 7:3). FTIR (cm^{-1}): 2037, 1912 (C═O); 1334, 1146 (S═O); 832 (S—N). ^{1}H NMR (400 MHz, DMSO d_6) δ (ppm): 9.13 (s, 1H), 8.89 (d, *J* = 5.3 Hz, 2H, H6/6′), 8.45 (d, *J* = 8.8 Hz, 1H), 8.34 (d, *J* = 8.2 Hz, 1H), 8.27 (m, 2H), 8.00 (t, 2H, H4/4′), 7.94 (t, 1H), 7.87 (t, 1H), 7.47 (t, 2H, H5/5′), 7.46 (d, 2H, H3/3′), 5.67 (d, *J* = 16.1 Hz, 2H, CH_2), 4.59 (d, *J* = 16.1 Hz, 2H, CH_2).

*2.2.4. Synthesis of [Re(CO)$_3$(N(SO_2Me_2Nnap)dpa)]PF$_6$ (**C3**)*

The above described method with 5-(dimethylamino)naphthalene-1-sulfonyl chloride (0.68 g) and *N*(H)dpa yielded the *N*(SO_2Me_2Nnap)dpa ligand as a brown oil. Slow evaporation of a solution of the obtained compound in acetone produced yellow needle-like crystals (1.01 g, 93% yield). R_f = 0.18 (dichloromethane/hexane 7:3). FTIR (cm^{-1}): 1322, 1140 (S═O); 918 (S—N). Treatment of the ligand (0.043 g) with [Re(CO)$_3$(H_2O)$_3$]$^+$ (1.00 ml) yielded [Re(CO)$_3$(N(SO_2Me_2Nnap)dpa)]PF$_6$ (0.055 g, 70% yield). R_f = 0.25 (ethyl acetate). FTIR (cm^{-1}): 2036, 1907 (C═O); 1358, 1143 (S═O); 866 (S—N). ^{1}H NMR data of the N(SO_2Me_2-Nnap)dpa ligand and [Re(CO)$_3$(N(SO_2Me_2Nnap)dpa)]PF$_6$ matched with the previously reported data [45].

2.3. Biological studies

2.3.1. Prediction of drug-likeness

The drug-likeness of the ligands synthesized in this study was determined by evaluating the properties stated in Lipinski's 'rule of 5′ [47]. The parameters mentioned in the 'rule of 5′ are molecular weight (MW), the number of hydrogen bond donors and acceptors and the logarithm of the octanol/water partition coefficient (LogP). Furthermore, properties such as molecular weight, hydrogen bond acceptors, hydrogen bond donors, water partition coefficient, molecular polar surface area and number of rotatable bonds were calculated via ChemAxon (www.chemicalize.org) [48] and molinspiration (www.molinspiration.com) [49] servers.

2.3.2. Identification of potential targets

The potential targets of the three ligands were predicted via SwissTargetPrediction (www.swisstargetprediction.ch) [50]. With SwissTargetPrediction, it is possible to identify proteins which interact with known molecules that are similar to the molecule of interest. It provides results including the predicted targets of diverse species, target classes, common names, the similarity between the ligand and all the known small molecules in the database and the prediction probability. The server also provides valuable information on how to modify the ligand in order to increase its biological activity by comparing the ligand with known similar molecules.

2.3.3. In vitro cytotoxicity assay

Isolation of human leukocytes was done using Histopaque-1077, as described in the standard protocol [51]. The viability of the leukocytes was determined by the Trypan blue dye exclusion method using a haemocytometer. The cells were incubated for 30 min with each compound using increasing concentrations at 37 °C. Each assay was carried out in triplicate and the mean viability of the leukocytes after treatment with the compounds was calculated.

2.3.4. Fluorescence micrographs

Allium cepa bulb cells and isolated human leukocytes were treated with each compound at their maximum tolerable concentrations (5 mg ml^{-1} solution of *N*(SO_2)(1-nap)dpa (**L1**), 1.25 mg ml^{-1} solutions of *N*(SO_2)(2-nap)dpa (**L2**), *N*(SO_2Me_2Nnap)dpa (**L3**) and [Re(CO)$_3$L2)]PF$_6$ (**C2**); 10 mg ml^{-1} solutions of [Re(CO)$_3$L1)]PF$_6$ (**C1**) and [Re(CO)$_3$L3)]PF$_6$ (**C3**) dissolved in DMSO-PBS buffer (4:1) solution). The cells were incubated for 10 min at room temperature

and observed under an Olympus BX51 epifluorescence microscope. Fluorescent micrographs were captured with an Olympus DP-70 camera and analyzed using Olympus Stream software.

2.3.5. Molecular docking studies

The binding affinity of the ligands to Prostaglandin G/H synthase 2 and Bovine Serum Albumin (BSA) was calculated using AutoDock Vina [52] wizard in the PyRx 0.8 software. The ligand structures were converted into PDB format using Avogadro 1.0.1. The protein structures were obtained in PDB format from the RCSB protein data bank (https://www.rcsb.org/structure/5KIR and https://www.rcsb.org/structure/6QS9) and prepared for molecular docking. The PDBQT files of the ligands were manually altered to assign the pyridyl nitrogen atom as an aromatic nitrogen atom. Blind docking was carried out to determine the specific binding pockets and binding affinity of the ligands to the selected proteins. Visualization of the conformations was done using the Discovery Studio software.

3. Results and discussion

The synthesis of the ligands **L1** and **L2**, as well as the crystal structures of all three ligands including **L3** which is described elsewhere [45], are reported herein. The two novel metal complexes reported in this study are examples of tertiary sulfonamide linear tridentate ligands bound to the *fac*-$[Re(CO)_3]^+$ core. Both the ligands and the corresponding metal complexes were synthesized in good yield and the completion of the reactions was monitored by TLC analysis as well as by UV–Visible analysis.

3.1. X-ray characterization

The crystal structures of the synthesized ligands provided evidence for the formation of a bond between the sulfonyl chloride and dpa moieties, as shown in the ORTEP of the ligands drawn at 50% probability (Fig. 2). The crystal structures of the ligands **L1**, **L2** and **L3**, crystallized from dichloromethane, were determined using diffraction data collected at low temperature on a Bruker Kappa Apex-II diffractometer using MoKα (**L1** and **L2**) or CuKα (**L3**) radiation. Absorption corrections were applied using the multi-scan method. Hydrogen atoms were visible in difference maps, but were placed in idealized positions and treated as riding in the refinements. The crystals of **L3** were small, weakly scattering 3-component twins, and refinement was versus a TWIN4 file produced by TWINABS. The twin fractions were estimated to be 59:34:7. Crystal data and refinement parameters are given in Table 1. The structural data have been deposited with the Cambridge Crystallographic Data Centre under deposition numbers CCDC 1961664–6. The S—N bond lengths of **L1**, **L2** and **L3** (1.6321(5), 1.6277(10) and 1.614(3) Å, respectively) are within the accepted range for sulfonamide bond values reported in previous studies [32]. The S═O, C—S and C—N bond lengths of the ligands lie within the normal range [53]. The bond angles around the N2 atom (C6-N2-C7, C6-N2-S1 and C7-N2-S1) are ~120° (Table 2) and therefore a trigonal planar geometry is observed around the N2(sp^2) nitrogen atom.

3.2. ^{1}H NMR characterization

The ^{1}H NMR spectra of the ligands and the metal complexes were recorded in DMSO d_6 and the peaks were assigned to the structures of the ligands and the corresponding Re complexes (Fig. 3). The aromatic protons of the ligands were observed in the region δ 7.09–8.6 ppm. All the peaks of the spectra of the ligands have been deshielded upon binding to the metal precursor due to electron withdrawing inductive effect of the metal. The singlet peak in each spectrum of the free ligands **L1**, **L2** and **L3** (at δ 4.7, 4.6 and 4.69 ppm, respectively) for the methylene protons appears as two doublets (*endo*- and *exo*-CH) in the spectra of the corresponding metal complexes (Table 3) as the methylene protons orient magnetically non-equivalent protons upon binding the metal precursor.

3.3. FT-IR spectroscopy

The spectroscopic data of the metal complexes were compared with the corresponding data of their ligands to confirm the formation of the metal complexes (Table 4). In the FTIR spectra of the $[Re(CO)_3L]^+$ complexes, two strong absorption peaks between 2025 and 1912 cm^{-1} are attributed to the stretching vibrations of the

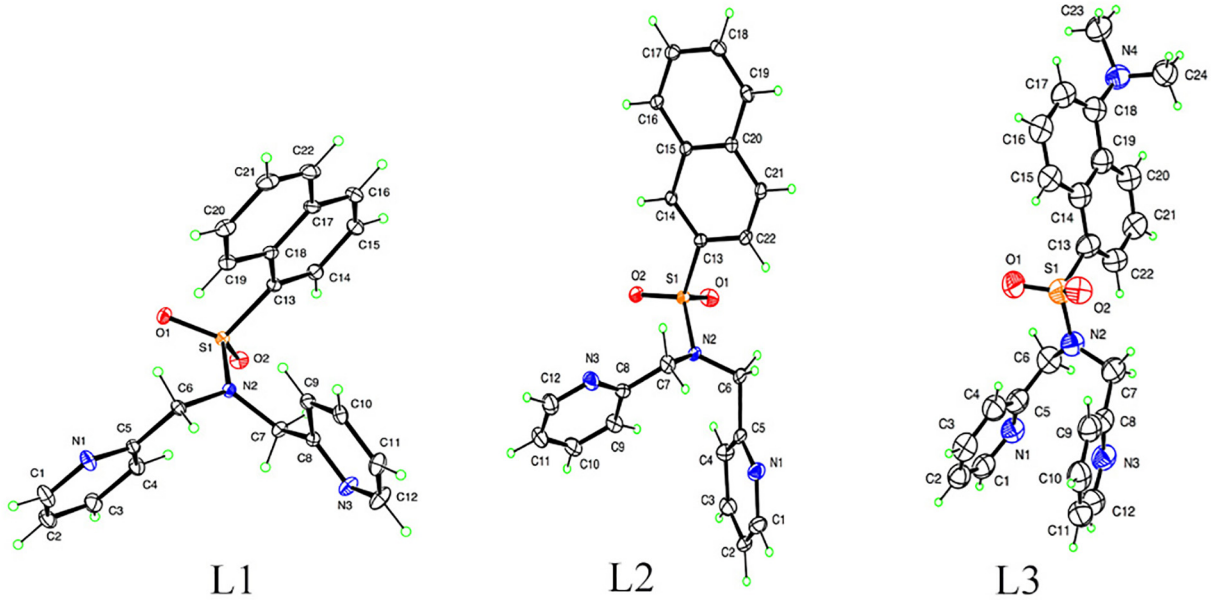

Fig. 2. ORTEPs of the ligands: $N(SO_2)$(1-nap)dpa (**L1**), $N(SO_2)$(2-nap)dpa (**L2**), $N(SO_2Me_2Nnap)$dpa (**L3**). Thermal ellipsoids are drawn at the 50% probability level.

Table 1
Crystal data and structural refinement parameters for $N(SO_2)$(1-nap)dpa (**L1**), $N(SO_2)$(2-nap)dpa (**L2**) and $N(SO_2Me_2Nnap)$dpa (**L3**).

	L1	L2	L3
Empirical formula	$C_{22}H_{19}N_3O_2S$	$C_{22}H_{19}N_3O_2S$	$C_{24}H_{24}N_4O_2S$
Deposition number	CCDC 1961664	CCDC 196165	CCDC 1961666
Formula weight	389.46	389.46	432.53
Radiation wavelength (Å)	0.71073	0.71073	1.54184
Crystal system	Monoclinic	Monoclinic	Triclinic
Space group	$P2_1/n$	$P2_1/n$	P-1
Unit cell dimensions			
a (Å)	9.8660(3)	20.8812(7)	9.8550(7)
b (Å)	13.3371(5)	5.6639(2)	10.2883(8)
c (Å)	13.9301(5)	17.2000(5)	11.6138(9)
α (deg)	–	–	101.999(5)
β (deg)	93.001(2)	114.172(2)	101.451(5)
γ (deg)	–	–	107.858(5)
V (Å^3)	1830.46(11)	1855.87(11)	1051.91(14)
T (K)	100	100	90
Z	4	4	2
density (Mg m^{-3})	1.413	1.394	1.366
F(0 0 0)	816	816	456
abs coeff (mm^{-1})	0.20	0.20	1.61
crystal size (mm)	0.36 × 0.30 × 0.21	0.37 × 0.19 × 0.05	0.18 × 0.12 × 0.10
$2\theta_{max}$(deg)	74.2	66.4	122.6
R_{int}	0.021	0.041	0.220
$R[F^2 > 2\sigma(F^2)]$	0.030	0.045	0.081
w$R(F^2)$	0.090	0.118	0.240
res. dens (e Å^{-3})	−0.33, 0.62	−0.29, 0.55	−0.62, 0.68
data/param	9336/253	7043/253	3234/282

Table 2
Selected bond lengths/Å and bond angles/° for $N(SO_2)$(1-nap)dpa (**L1**), $N(SO_2)$(2-nap)dpa (**L2**) and $N(SO_2Me_2Nnap)$dpa (**L3**).

	L1	L2	L3
S1-N2	1.6321(5)	1.6277(10)	1.614(3)
N2-C6	1.4605(7)	1.4742(16)	1.455(5)
N2-C7	1.4646(7)	1.4714(16)	1.480(6)
N1-C1	1.3407(9)	1.3488(18)	1.348(5)
N1-C5	1.3420(8)	1.3327(17)	1.345(5)
N3-C8	1.3432(8)	1.3408(17)	1.344(5)
N3-C12	1.3410(9)	1.3372(19)	1.342(6)
S1-C13	1.7706(6)	1.7699(12)	1.782(4)
S1-O1	1.4384(5)	1.4338(10)	1.436(3)
S1-O2	1.4386(5)	1.4331(10)	1.430(3)
C5-N1-C1	117.60(6)	116.76(12)	116.2(3)
C12-N3-C8	117.27(6)	117.66(12)	116.2(4)
C6-N2-C7	118.90(5)	117.23(10)	117.2(3)
C6-N2-S1	120.33(4)	119.48(9)	119.9(3)
C7-N2-S1	118.42(4)	115.70(8)	121.2(3)

carbonyl ligands of the $Re(CO)_3$ core [3] and these peaks have shifted to a lower frequency in comparison with those of the precursor $[Re(CO)_3(H_2O)_3]$OTf (1914 and 2036 cm^{-1}). The three carbonyl stretching frequencies confirmed the facial geometry of the Re complexes [54]. Peaks due to S—N stretching vibrations, observed at 916–929 cm^{-1} in **L1**-**L3**, have shifted to lower wavenumbers in the respective metal complexes as the donation of the lone pair electrons on the sp^2 hybridized sulfonamide nitrogen atom lowers the initial S—N bond energy. The vibration bands due to asymmetric and symmetric stretching vibrations of the sulfonamide groups of the compounds are clearly visible in the regions 1321–1371 and 1131–1164 cm^{-1} (Table 4). The broad peak that appears at 3331 cm^{-1} in the spectrum of $[Re(CO)_3(H_2O)_3]$OTf cannot be seen in the spectrum of the complex, which confirms the formation of a bond with the ligand.

3.4. UV–Visible and fluorometric analysis

The UV–Visible spectra were recorded from 200 to 500 nm for all six compounds (Fig. S1). The higher energy band observed at 230 nm for **L1** was attributed to intra-ligand transitions ($n \rightarrow \pi^*$ and $\pi \rightarrow \pi^*$) which could arise from the heterocyclic, conjugated aromatic structure of the ligand. The absorption spectrum of **C1** shows a bathochromic shift compared to its free ligand, with an intense absorption band at 247 nm and two shoulder bands at 217 and 269 nm. The lower energy band in the region 320–350 nm was attributed to a metal to ligand charge transfer (MLCT) transition. The assignments of these peaks are in good agreement with the previously reported results for $[Re(bcp)(CO)_3(4\text{-}COOHPy)](ClO_4)$ [55].

The absorption spectrum of **C2** shows a hypsochromic shift compared to the spectrum of **L2**. Three absorption bands could be observed in the UV spectrum of **L3** at 217, 256 and 342 nm. The band at 256 nm was ascribed to charge transfer transitions (CT) involving the dimethylamino moiety as a donor and the dansyl group as an acceptor, while the band at 342 nm was ascribed to a CT transfer in the dansyl group [56]. Dansyl derivatized compounds are reported to have a twisted intramolecular charge transfer (TICT), in which the *N*-amine group behaves as the donor group and the naphthyl group behaves as the acceptor [57]. Upon binding to the Re atom, the band at 342 nm has shifted and broadened as a result of a MLCT (metal to ligand charge transfer) transition.

The small shoulder band, appearing at 260 nm in the spectra of **L1**, **C1**, **L2** and **C2**, was used to excite the compounds and get emission spectra (Fig. 4). The lower fluorescence intensities of **C1** and **C2** in comparison with those of the free ligands **L1** and **L2** may be due to quenching of fluorescence upon direct binding of the sulfonamide nitrogen atom to the Re metal atom.

The **L3** ligand and its Re complex were excited at 339 nm and the emission spectra were obtained in methanol (Fig. 4). A single, broad emission band for **L3** was observed in the 500–600 nm region. As in the other compounds used in this study, **L3** and **C3** show a concentration dependence of the fluorescence intensity, in which at lower concentrations, the fluorescence intensity increases when the concentration of the compound increases. However, for **L3** and **C3**, after a certain point, upon increasing the concentration of the compounds, the fluorescence intensity starts decreasing, possibly due to an inner filter effect [58]. As expected, the fluorescence intensity is quenched after binding the ligand **L3** to the tricarbonyl Re(I) moiety.

The emission spectra of all the synthesized compounds except **C1** show remarkable fluorescence intensities, and thus may be investigated further in bioimaging applications. Ranasinghe et al. (2016) has reported that even the quenched fluorescence intensity could be enhanced once the compound is bound to biomolecules in a cellular environment [25]. The Stokes shifts for the compounds were calculated using the emission and excitation maxima obtained from the spectra.

$$\Delta\lambda_S = \lambda_{max}(\text{emission}) - \lambda_{max}(\text{absorbance})$$

According to the results, the Stokes shifts for **L1**, **L2**, **L3**, **C1**, **C2** and **C3** are 116, 113, 308, 126, 78 and 326 nm, respectively (Table 5). **C3** possesses the largest Stokes shift among the compounds, which makes it favourable for a fluorescent dye.

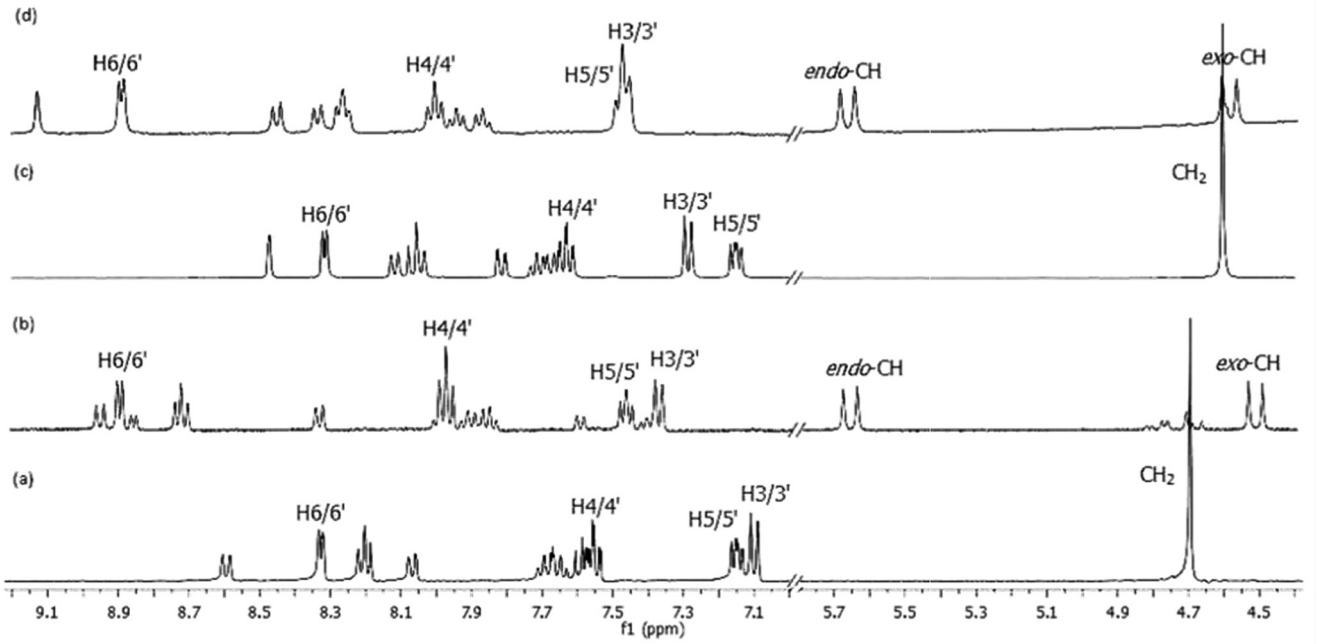

Fig. 3. ^{1}H NMR spectra of $N(SO_2)$(1-nap)dpa (a), $[Re(CO)_3(N(SO_2)(1\text{-nap})dpa)]PF_6$ (b), $N(SO_2)$(2-nap)dpa (c) and $[Re(CO)_3(N(SO_2)(2\text{-nap})dpa)]PF_6$ (d) in DMSO d_6 at 25 °C.

Table 3
Comparison of ^{1}H NMR shifts (δ, ppm) of selected peaks of the synthesized compounds in DMSO d_6 at 25 °C.

	H6/6′	H5/5′	H4/4′	H3/3′	CH_2
$N(SO_2)$(1-nap)dpa	8.32	7.15	7.55	7.10	4.70
$[Re(CO)_3(N(SO_2)(1\text{-nap})dpa)]PF_6$	8.90	7.47	7.98	7.37	5.66, 4.52
$\Delta\delta$ (ppm) of **C1**	(+) 0.58	(+) 0.32	(+) 0.43	(+) 0.27	
$N(SO_2)$(2-nap)dpa	8.32	7.15	7.63	7.29	4.60
$[Re(CO)_3(N(SO_2)(2\text{-nap})dpa)]PF_6$	8.89	7.47	8.00	7.46	5.67, 4.59
$\Delta\delta$ (ppm) of **C2**	(+) 0.57	(+) 0.32	(+) 0.37	(+) 0.17	
$N(SO_2Me_2Nnap)dpa$	8.33	7.15	7.53–7.59	7.09	4.69
$[Re(CO)_3(N(SO_2Me_2Nnap)dpa)]PF_6$	8.92–8.89	7.49–7.39	8–7.92	7.49–7.39	5.63, 4.53

Table 4
The characteristic IR peaks of the ligands and their metal complexes in cm^{-1}.

Ligand/Complex	νS-N	$\nu_{as}(SO_2)$	$\nu_s(SO_2)$	ν(CO)
L1	917	1321	1131	
C1	808	1371	1164	2025, 1899
L2	928	1334	1146	
C2	832	1334	1146	2037, 1912
L3	918	1322	1140	
C3	866	1358	1143	2036, 1907

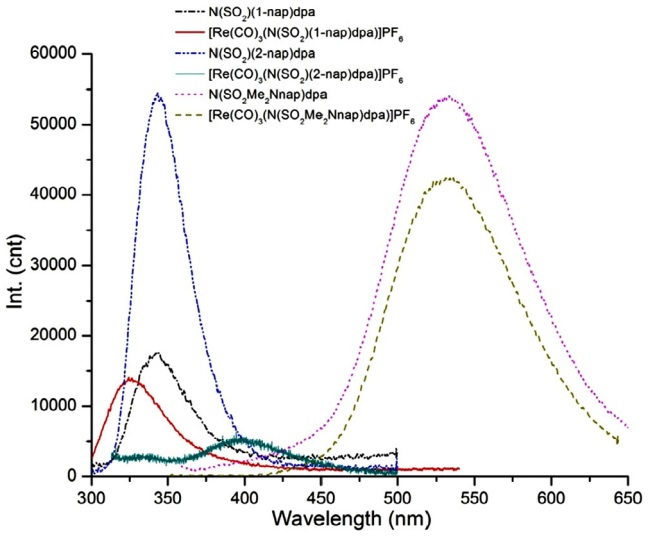

Fig. 4. Fluorescence spectra of $N(SO_2)$(1-nap)dpa (0.1 mM), $[Re(CO)_3(N(SO_2)(1\text{-nap})dpa)]PF_6$ (0.1 mM), $N(SO_2)$(2-nap)dpa (0.1 mM), $[Re(CO)_3(N(SO_2)(2\text{-nap})dpa)]PF_6$ (0.1 mM), $N(SO_2Me_2Nnap)dpa$ (0.01 mM) and $[Re(CO)_3(N(SO_2Me_2Nnap)dpa)]PF_6$ (0.1 mM) in methanol at 298 K.

3.5. Biological studies

3.5.1. Prediction of drug-likeness

Solubility and membrane permeability of a compound should be tested when designing a new drug and it should not violate the 'rule of 5' for it to be an orally active drug. Such compounds should possess MW $\leq$ 500, logP $\leq$ 5, hydrogen bond donors $\leq$ 5, hydrogen bond acceptors $\leq$ 10, polar surface area $\leq$ 150 Å^2 and rotatable bonds $\leq$ 10 [59]. These parameters were calculated via ChemAxon (https://chemaxon.com/) and Molinspiration (https://www.molinspiration.com) servers and the results revealed that all the parameters mentioned above are within the range for the three ligands reported in this study (Supporting Information, Table S1) with zero violations which indicates their potential applicability as drug leads.

Table 5
Photophysical properties of the synthesized compounds in methanol.

Test sample	Excitation wavelength/nm	Emission wavelength/nm	Fluorescence Quantum yield	$\Delta\lambda_S$/nm
$N(SO_2)$(1-nap)dpa	260	338	0.056	116
$[Re(CO)_3(N(SO_2)$(1-nap)dpa)]PF_6	260	335	–	126
$N(SO_2)$(2-nap)dpa	260	343	0.039	113
$[Re(CO)_3(N(SO_2)$(2-nap)dpa)]PF_6	260	325	–	78
$N(SO_2Me_2N$nap)dpa	339	525	–	308
$[Re(CO)_3(N(SO_2Me_2N$nap)dpa)]PF_6	339	535	–	326

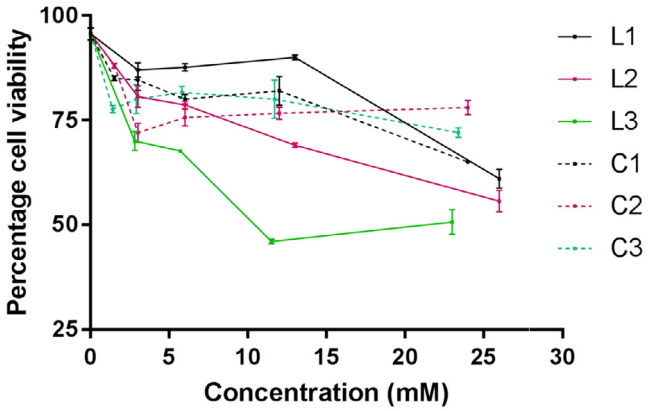

Fig. 5. Percentage cell viability of human lymphocytes incubated in compounds **L1**, **L2**, **L3**, **C1**, **C2** and **C3** at different concentrations (mM).

3.5.2. Identification of potential targets

Target prediction by SwissTargetPrediction (http://www.swisstargetprediction.ch) revealed that the ligands can be prostaglandin G/H synthase 2 inhibitors. Prostaglandin G/H synthase 2 (COX2 or Cyclooxygenase-2) is induced with inflammation in mammalian species [60] and belongs to the target class of oxidoreductase. Anti-inflammatory drugs inhibit the activity of the Prostaglandin enzyme. The server predicts a probability of 6.7% for **L1**, **L2** and **L3** to have oxidoreductase as biotargets.

3.5.3. In vitro cytotoxicity assay

The cytotoxicity and cellular uptake properties of the synthesized compounds were investigated against human lymphocytes [61]. The compounds were dissolved in DMSO:PBS (4:1) solution as the compounds are not soluble in water. We did not observe significant toxicity against cells due to the DMSO solutions used in the study. The viable cell count of the cells incubated with the free

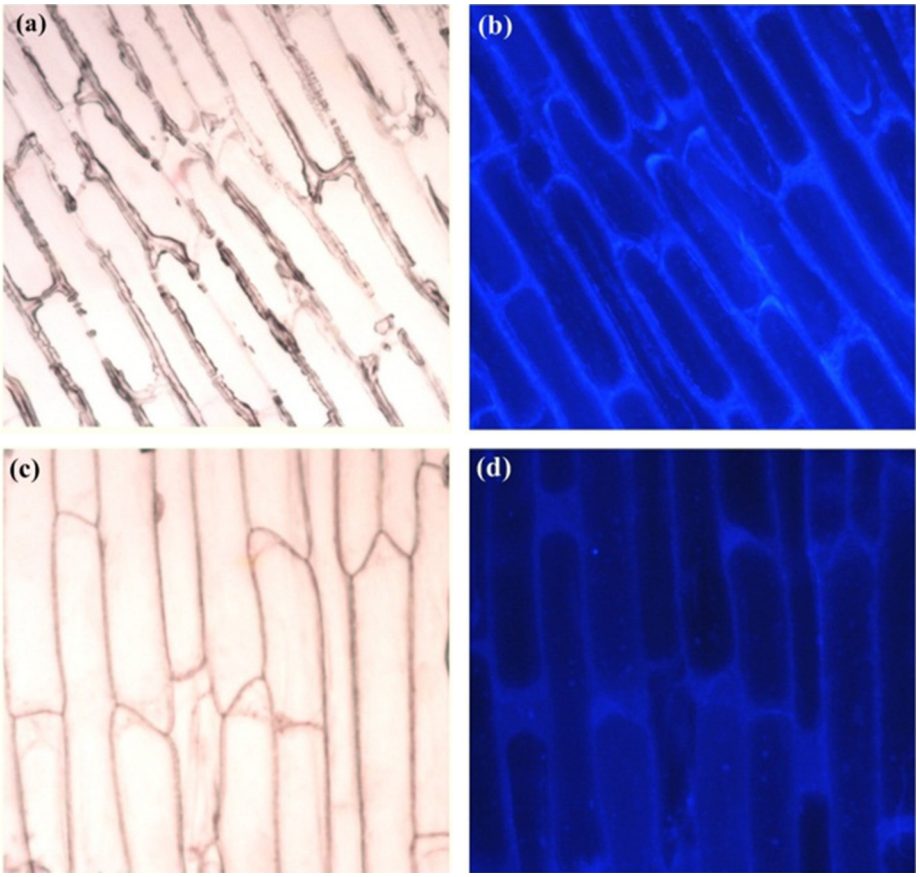

Fig. 6. Micrographs of *Allium cepa* bulb cells incubated with 0.003 M of $N(SO_2Me_2N$nap)dpa (**L3**) in DMSO solution under an optical microscope (a), under an epifluorescence microscope (b). Micrographs of *Allium cepa* bulb cells incubated with 0.012 M of $[Re(CO)_3$L3]PF_6 (**C3**) in DMSO solution under an optical microscope (c), under an epifluorescence microscope (d).

ligands could not be determined at a higher concentration than 26 mM due to the water insolubility.

The toxicity to cells increases with the ligand concentration for **L2** and **L3**. However, **L1** is observed to have no significant toxicity up to 13 mM and the cell viability is in the range of 87 to 90% (Fig. 5). The compounds were not toxic in the tested range of concentrations, therefore the IC_{50} values of the compounds were not determined. The reported compounds are well tolerated by mammalian cells at their highest soluble concentration. This is a desirable character for a drug lead which seeks a specific activity.

3.5.4. Fluorescence microscopy

The three ligands revealed good fluorescence properties which led us to study further the cellular uptake of the compounds to assess their potential to be utilized as bioimaging agents. When incubated with *Allium cepa* bulb cells, increased fluorescence was detected around the cells where the cell wall accumulated the compound. Fluorescence images taken for the compounds **L1**, **L2**, **C1** and **C2** did not show any focal concentrations that would enhance the fluorescence inside plant cells and human lymphocytes and, therefore, the compounds are not effective fluorophores for the tested cell types. The conjugated, aromatic structure of the dansyl group in **L3** and **C3** is expected to exhibit enhanced emission intensities, which is good in bioimaging applications as the tissue penetration ability increases [23]. Plant cells illuminated after treatment with **L3** and **C3** produced images at the maximum tolerable concentrations, but the cellular uptake of the compounds is not clear (Fig. 6). However, local accumulation in the cell walls showed contrasting fluorescence around the plant cells. Since fluorescence microscopy does not show distinct focal points of fluorescence, it is not a suitable method to determine the cellular uptake of these compounds.

3.5.5. Molecular docking studies

Preliminary docking studies were carried out to evaluate the ligands' binding to prostaglandin synthase 2 (Fig. 7). Docking studies revealed that **L1** binds to the prostaglandin protein with a binding affinity of −9.0 kcal/mol, while **L2** binds to the protein with a calculated binding energy of −8.7 kcal/mol (Fig. 8). Both ligands bind to pockets in the dimer interface, suggesting changes that

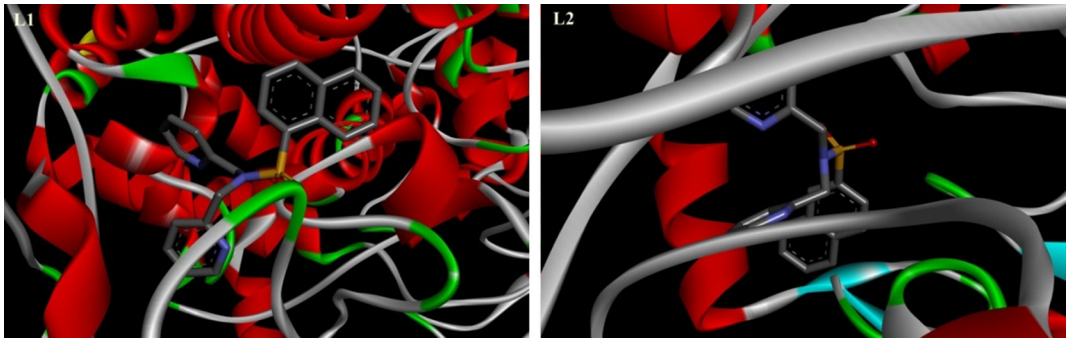

Fig. 7. Molecular docked structures of the ligands **L1** and **L2** with Prostaglandin synthase 2.

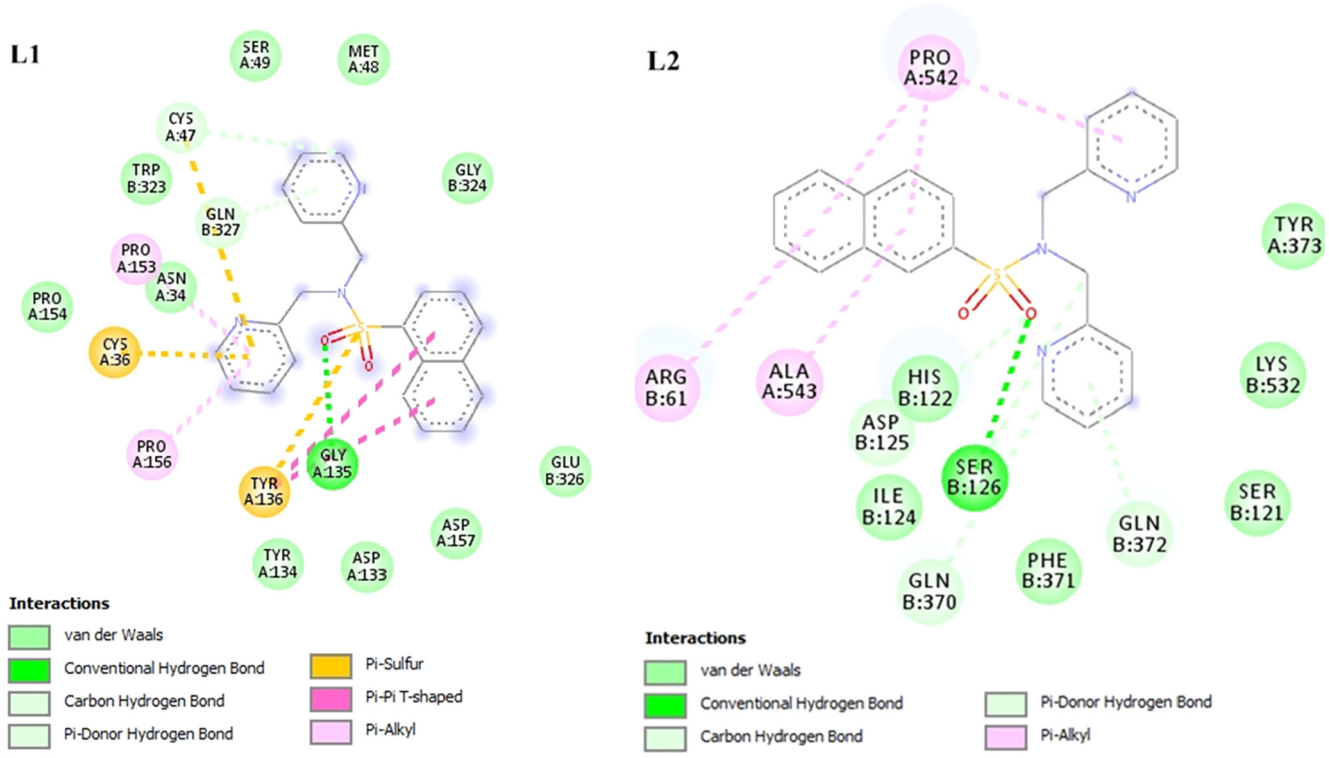

Fig. 8. Bonding interactions of the ligands **L1** and **L2** with Prostaglandin synthase 2.

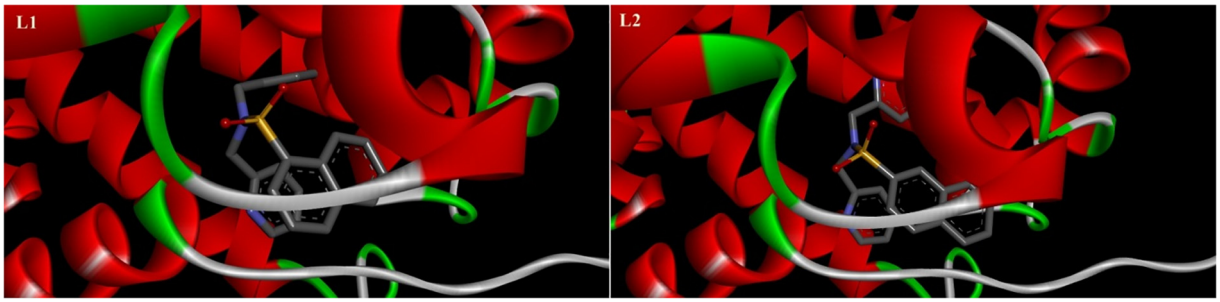

Fig. 9. Molecular docked structures of the ligands **L1** and **L2** with BSA.

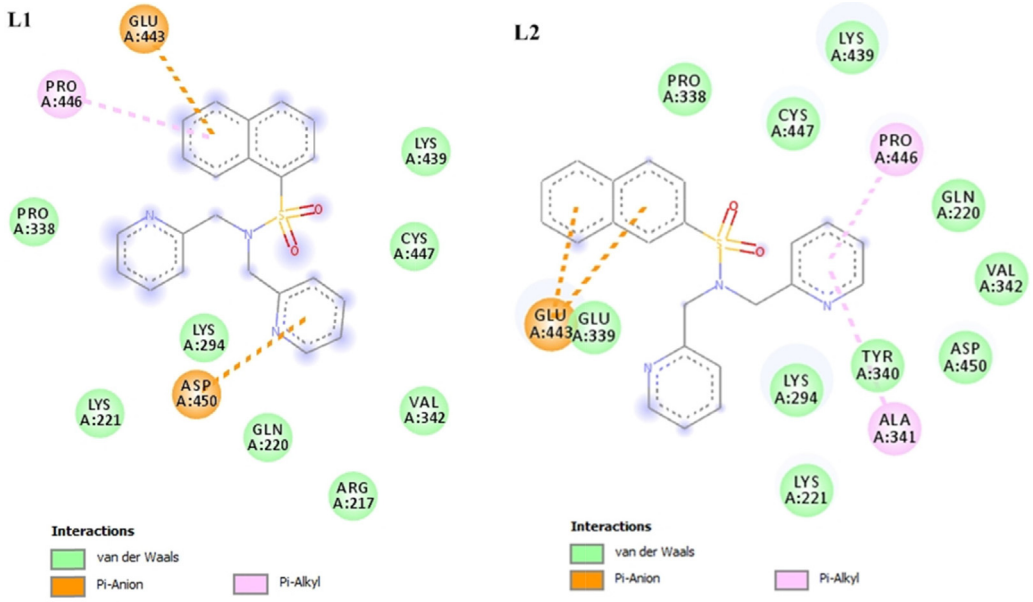

Fig. 10. Bonding interactions of the ligands **L1** and **L2** with BSA.

would affect the global conformation and the activity of the protein.

Serum albumins play a major role in distributing drugs in the body. Further to support their drug-like nature, we analyzed their binding to Bovine Serum Albumin (BSA). The ligands were docked in specific binding pockets in BSA with thermodynamically favourable binding energies, indicating the possibility of interaction leading to serum distribution (Figs. 9 and 10). The ligands **L1** and **L2** interact with BSA with predicted binding energies of −6.2 and −7.0 kcal/mol, respectively.

4. Conclusions

In conclusion, we have synthesized and characterized three dipicolylamine-based ligands and their corresponding rhenium(I) complexes. This study has examined the photophysical properties and the capability of the compounds to be utilized as anti-inflammatory drug leads.

The formation of the three ligands was confirmed by spectroscopic measurements, including ^{1}H NMR and X-ray crystallographic analysis. We report the single crystal structure and structural refinement data for **L1**-**L3**. We also present UV–Vis, FTIR and emission spectroscopy data for all six compounds. The absorption spectrum of **C1** shows a bathochromic shift while **C2** shows a hypsochromic shift compared to the free ligands. The metal to ligand charge transfer (MLCT) transitions of **C1** and **C3** lie in the region 320–350 nm. The three ligands agree with the Lipinski's rule of 5 and the drug-likeness properties evaluated by ChemAxon and Molinspiration servers confirmed their potential bio applicability as drug leads. To further support the results obtained by SwissTargetPrediction, the binding ability of the ligands to BSA was studied through molecular docking and the results indicate a high serum distribution for all three ligands. Specific binding modes of the ligands to prostaglandin synthase 2 suggests that the ligands are probable inhibitors and could be further studied as suitable compounds to act as anti-inflammatory agents. Cytotoxicity was tested for all six compounds on *Allium cepa* bulb cells and human lymphocytes. The compounds were not toxic to human lymphocytes at their highest soluble concentration. Remarkably higher fluorescence intensities were given for compounds **L1**, **L2**, **L3**, **C2** and **C3** at 10 μM concentration. **L3** and **C3** showed a concentration dependence of the maximum fluorescence intensity. Unfortunately, the fluorescent studies were not conclusive for cellular uptake and further studies are warranted to ascertain the cellular uptake of the compounds.

CRediT authorship contribution statement

Taniya Darshani: Investigation, Formal analysis, Methodology, Writing - original draft. **Nadini Thushara**: Formal analysis, Methodology, Data curation. **Piyumali Weerasuriya**: Formal analysis. **Frank R. Fronczek**: Investigation, Resources, Formal analysis,

Data curation. **Inoka C Perera**: Investigation, Resources, Formal analysis. **Theshini Perera**: Methodology, Conceptualization, Supervision, Writing - review & editing.

Declaration of Competing Interest

The authors declare that they have no known competing financial interests or personal relationships that could have appeared to influence the work reported in this paper.

Acknowledgements

This work was supported by Grant no ASP/01/RE/SCI/2018/38 of the University of Sri Jayewardenepura, Sri Lanka with the support for instrumentation from the Instrument Centre and Centre for Advanced Material Research of the University of Sri Jayewardenepura. The authors thank Imesha Lakmini Hettige for helping with the docking studies.

Author contributions

TD carried out the synthesis, purification and characterization of the compounds, as well as initial writing of manuscript. NT synthesized and purified the ligand **L2**. PW carried out the docking studies together with TD. TP designed and conceived the study and finalized the manuscript. ICP designed the biological experiments. FRF carried out the X-ray data collection and structure determination. All authors read and approved the final manuscript.

Appendix A. Supplementary data

CCDC 1961664–6 contains the supplementary crystallographic data for *N*(SO_2)(1-nap)dpa, *N*(SO_2)(2-nap)dpa and *N*(SO_2Me_2-Nnap)dpa. These data can be obtained free of charge via http://www.ccdc.cam.ac.uk/conts/retrieving.html or from the Cambridge Crystallographic Data Centre, 12 Union Road, Cambridge CB2 1EZ, UK; fax: (+44) 1223-336-033; or e-mail: deposit@ccdc.cam.ac.uk. Supplementary data to this article can be found online at https://doi.org/10.1016/j.poly.2020.114592.

References

[1] A. Leonidova, G. Gasser, Underestimated potential of organometallic rhenium complexes as anticancer agents, ACS Chem. Biol. 9 (10) (2014) 2180–2193.
[2] S. Rafique, M. Idrees, A. Nasim, H. Akbar, A. Athar, Transition metal complexes as potential therapeutic agents, Biotechnol. Mol. Biol. Rev. 5 (2) (2010) 38–45.
[3] S.K. Bharti, S.K. Singh, Recent developments in the field of anticancer metallopharmaceuticals, Int. J. PharmTech Res. 1 (2009) 1406–1420.
[4] E. Baggaley, J.A. Weinstein, J.G. Williams, Lighting the way to see inside the live cell with luminescent transition metal complexes, Coord. Chem. Rev. 256 (15–16) (2012) 1762–1785.
[5] V. Fernandez-Moreira, F.L. Thorp-Greenwood, M.P. Coogan, Application of d6 transition metal complexes in fluorescence cell imaging, Chem. Commun. 46 (2) (2010) 186–202.
[6] K. Tanaka, K. Fukase, PET (positron emission tomography) imaging of biomolecules using metal–DOTA complexes: a new collaborative challenge by chemists, biologists and physicians for future diagnostics and exploration of in vivo dynamics, Org. Biomol. Chem. 6 (5) (2008) 815–828.
[7] Radioisotopes I, No RS. Technetium-99m Radiopharmaceuticals: Status and Trends. Vienna; 2009.
[8] R.K. Hom, J.A. Katzenellenbogen, Technetium-99m-labeled receptor-specific small-molecule radiopharmaceuticals: recent developments and encouraging results, Nucl. Med. Biol. 24 (6) (1997) 485–498.
[9] M. Gielen, E.R. Tiekink, Metallotherapeutic Drugs and Metal-Based Diagnostic Agents: The Use of Metals in Medicine, John Wiley & Sons, 2005.
[10] M. Rey, A., Radiometal complexes in molecular imaging and therapy, Curr. Med. Chem. 17 (31) (2010) 3673–3683.
[11] D.K. Emerson, K.K. Limmer, D.J. Hall, S.-H. Han, W.C. Eckelman, C.J. Kane, A.M. Wallace, D.R. Vera, A receptor-targeted fluorescent radiopharmaceutical for multireporter sentinel lymph node imaging, Radiology 265 (1) (2012) 186–193.
[12] R. Alberto, H.P. N'Dongo, M. Clericuzio, S. Bonetti, E. Gabano, C. Cassino, M. Ravera, D. Osella, Functionalized thymidine derivatives as carriers for the γ-emitter technetium tricarbonyl moiety, Inorg. Chim. Acta 362 (13) (2009) 4785–4790.
[13] K.A. Stephenson, S.R. Banerjee, T. Besanger, O.O. Sogbein, M.K. Levadala, N. McFarlane, J.A. Lemon, D.R. Boreham, K.P. Maresca, J.D. Brennan, J.W. Babich, J. Zubieta, J.F. Valliant, Bridging the gap between in vitro and in vivo imaging: isostructural Re and 99mTc complexes for correlating fluorescence and radioimaging studies, J. Am. Chem. Soc. 126 (28) (2004) 8598–8599.
[14] K.K.W. Lo, K.Y. Zhang, S.P.Y. Li, Recent exploitation of luminescent rhenium (I) tricarbonyl polypyridine complexes as biomolecular and cellular probes, Eur. J. Inorg. Chem. 24 (2011) 3551–3568.
[15] A.J. Amoroso, M.P. Coogan, J.E. Dunne, V. Fernández-Moreira, J.B. Hess, A.J. Hayes, D. Lloyd, C. Millet, S.J.A. Pope, C. Williams, Rhenium fac tricarbonyl bisimine complexes: biologically useful fluorochromes for cell imaging applications, Chem. Commun. 29 (2007) 3066–3068.
[16] R.G. Balasingham, F.L. Thorp-Greenwood, C.F. Williams, M.P. Coogan, S.J. Pope, Biologically compatible, phosphorescent dimetallic rhenium complexes linked through functionalized alkyl chains: syntheses, spectroscopic properties, and applications in imaging microscopy, Inorg. Chem. 51 (3) (2012) 1419–1426.
[17] P.V. Simpson, I. Casari, S. Paternoster, B.W. Skelton, M. Falasca, M. Massi, Defining the anti-cancer activity of tricarbonyl rhenium complexes: induction of G2/M cell cycle arrest and blockade of aurora-A kinase phosphorylation, Chem. Eur. J. 23 (27) (2017) 6518–6521.
[18] D. Hernández-Valdés, G. Meola, H. Braband, B. Spingler, R. Alberto, Direct synthesis of non-alkyl functionalized bis-arene complexes of rhenium and 99 (m) technetium, Organometallics 37 (17) (2018) 2910–2916.
[19] J. Dilworth, S. Parrott, The biomedical chemistry of technetium and rhenium, Chem. Soc. Rev. 27 (1) (1998) 43–55.
[20] M. Lipowska, H. He, X. Xu, A.T. Taylor, P.A. Marzilli, L.G. Marzilli, Coordination modes of multidentate ligands in fac-[$Re(CO)_3$(polyaminocarboxylate)] analogues of 99mTc radiopharmaceuticals. Dependence on aqueous solution reaction conditions, Inorg. Chem. 49 (7) (2010) 3141–3151.
[21] J.R. Dilworth, P.S. Donnelly, 75Re therapeutic rhenium radiopharmaceuticals. metallotherapeutic drugs and metal-based diagnostic agents: the use of metals in medicine. 2005: 463–87
[22] M.A. Wuillemin, M.J. Reber, T. Fox, B. Spingler, D. Brühwiler, R. Alberto, H. Braband, Towards 99mTc-and Re-based multifunctional silica platforms for theranostic applications, Inorganics 7 (11) (2019) 134.
[23] K.K.-W. Lo, Luminescent rhenium (I) and iridium (III) polypyridine complexes as biological probes, imaging reagents, and photocytotoxic agents, Acc. Chem. Res. 48 (12) (2015) 2985–2995.
[24] K.K.-W. Lo, A.W.-T. Choi, W.H.-T. Law, Applications of luminescent inorganic and organometallic transition metal complexes as biomolecular and cellular probes, Dalton Trans. 41 (20) (2012) 6021–6047.
[25] K. Ranasinghe, S. Handunnetti, I.C. Perera, T. Perera, Synthesis and characterization of novel rhenium (I) complexes towards potential biological imaging applications, Chem. Cent. J. 10 (1) (2016) 71.
[26] A.J. Amoroso, R.J. Arthur, M.P. Coogan, V. Fernández-Moreira, A.J. Hayes, D. Lloyd, C. Millet, S.J.A. Pope, 3-Chloromethylpyridyl bipyridine fac-tricarbonyl rhenium: a thiol-reactive luminophore for fluorescence microscopy accumulates in mitochondria, New J. Chem. 32 (7) (2008) 1097–1102.
[27] E. Ferri, D. Donghi, M. Panigati, G. Prencipe, L. D'Alfonso, I. Zanoni, C. Baldoli, S. Maiorana, G. D'Alfonso, E. Licandro, Luminescent conjugates between dinuclear rhenium (I) complexes and peptide nucleic acids (PNA) for cell imaging and DNA targeting, Chem. Commun. 46 (34) (2010) 6255–6257.
[28] A.M. Christoforou, F.R. Fronczek, P.A. Marzilli, L.G. Marzilli, fac-$Re(CO)_3$L Complexes containing tridentate monoanionic ligands (L-) with a seldom-studied sulfonamido group as one terminal ligating group, Inorg. Chem. 46 (17) (2007) 6942–6949.
[29] P.L. Abhayawardhana, P.A. Marzilli, F.R. Fronczek, L.G. Marzilli, Complexes possessing rare "tertiary" sulfonamide nitrogen-to-metal bonds of normal length: fac-[$Re(CO)_3(N(SO_2R)dien)]PF_6$ complexes with hydrophilic sulfonamide ligands, Inorg. Chem. 53 (2) (2014) 1144–1155.
[30] K.K.-W. Lo, M.-W. Louie, K.-S. Sze, J.S.-Y. Lau, Rhenium(I) polypyridine biotin isothiocyanate complexes as the first luminescent biotinylation reagents: synthesis, photophysical properties, biological labeling, cytotoxicity, and imaging studies, Inorg. Chem. 47 (2) (2008) 602–611.
[31] R.G. Balasingham, M.P. Coogan, F.L. Thorp-Greenwood, Complexes in context: Attempting to control the cellular uptake and localisation of rhenium fac-tricarbonyl polypyridyl complexes, Dalton Trans. 40 (44) (2011) 11663–11674.
[32] A. Subasinghe, I.C. Perera, S. Pakhomova, T. Perera, Synthesis, characterization, and biological studies of a piperidinyl appended dipicolylamine ligand and its rhenium tricarbonyl complex as potential therapeutic agents for human breast cancer, Bioinorg. Chem. Appl. 2016 (2016) 2675937.
[33] H. Agarwalla, N. Taye, S. Ghorai, S. Chattopadhyay, A. Das, A novel fluorescence probe for estimation of cysteine/histidine in human blood plasma and recognition of endogenous cysteine in live Hct116 cells, Chem. Commun. 50 (69) (2014) 9899–9902.
[34] M.M. Ibrahim, A.-M.M. Ramadan, G.A. Mersal, S.A. El-Shazly, Synthesis, superoxide dismutase, nuclease, and anticancer activities of copper(II) complexes incorporating bis (2-picolyl) amine with different counter anions, J. Mol. Struct. 998 (1–3) (2011) 1–10.

[35] T. Storr, C.L. Fisher, Y. Mikata, S. Yano, M.J. Adam, C. Orvig, A glucosamine–dipicolylamine conjugate of 99m Tc (i) and 186 Re (i) for use in imaging and therapy, Dalton Trans. 4 (2005) 654–655.
[36] F. Tay, C. Erkan, N.Y. Sariozlu, E. Ergene, S. Demirayak, Synthesis, antimicrobial and anticancer activities of some naphthylthiazolylamine derivatives, Biomed. Res. 28 (6) (2017) 2696–2703.
[37] M.H. Huang, S.N. Wu, J.P. Wang, C.H. Lin, S.I. Lu, L.F. Liao, A.Y. Shen, Biological study of naphthalene derivatives with antiinflammatory activities, Drug Dev. Res. 60 (4) (2003) 261–269.
[38] J. Chen, Y-w Huang, G. Liu, Z. Afrasiabi, E. Sinn, S. Padhye, Y. Ma, The cytotoxicity and mechanisms of 1, 2-naphthoquinone thiosemicarbazone and its metal derivatives against MCF-7 human breast cancer cells, Toxicol. Appl. Pharm. 197 (1) (2004) 40–48.
[39] S. Göksu, M. Tansu, H. Özdemir, H. Seçen, A concise synthesis and the antibacterial activity of 5, 6-dimethoxynaphthalene-2-carboxylic acid, Turk. J. Chem. 29 (2) (2005) 199–205.
[40] Y. Rokade, R. Sayyed, Naphthalene derivatives: A new range of antimicrobials with high therapeutic value, Rasayan J. Chem. 2 (4) (2009) 972–980.
[41] V.K. Tandon, R.B. Chhor, R.V. Singh, S. Rai, D.B. Yadav, Design, synthesis and evaluation of novel 1, 4-naphthoquinone derivatives as antifungal and anticancer agents, Bioorg. Med. Chem. Lett. 14 (5) (2004) 1079–1083.
[42] M. Yang, M. Sun, Z. Zhang, S. Wang, A novel dansyl-based fluorescent probe for highly selective detection of ferric ions, Talanta 105 (2013) 34–39.
[43] T.R. Lakshman, J. Deb, I. Ghosh, S. Sarkar, T.K. Paine, Combining anti-inflammatory and anti-proliferative activities in ternary metal-NSAID complexes of a polypyridylamine ligand, Inorg. Chim. Acta 48 (2019) 663–668.
[44] R. Aggarwal, A. Bansal, I. Rozas, B. Kelly, P. Kaushik, D. Kaushik, Synthesis, biological evaluation and molecular modeling study of 5-trifluoromethyl-Δ2-pyrazoline and isomeric 5/3-trifluoromethylpyrazole derivatives as anti-inflammatory agents, Eur. J. Med. Chem. 70 (2013) 350–357.
[45] T. Perera, P. Abhayawardhana, P.A. Marzilli, F.R. Fronczek, Marzilli LG. Formation of a metal-to-nitrogen bond of normal length by a neutral sufonamide group within a tridentate ligand. A new approach to radiopharmaceutical bioconjugation, Inorg. Chem. 52 (5) (2013) 2412–2421.
[46] H. He, M. Lipowska, X. Xu, A.T. Taylor, M. Carlone, L.G. Marzilli, $Re(CO)_3$ complexes synthesized via an improved preparation of aqueous fac-$[Re(CO)_3(H_2O)_3]^+$ as an aid in assessing 99mTc imaging agents. Structural characterization and solution behavior of complexes with thioether-bearing amino acids as tridentate ligands, Inorg. Chem. 44 (15) (2005) 5437–5446.
[47] C.A. Lipinski, F. Lombardo, B.W. Dominy, P.J. Feeney, Experimental and computational approaches to estimate solubility and permeability in drug discovery and development settings, Adv. Drug Deliv. Rev. 23 (1–3) (1997) 3–25.
[48] C. Southan, A. Stracz, Extracting and connecting chemical structures from text sources using chemicalize, J. Cheminf. 5 (1) (2013) 20.
[49] V. Karthick, K. Ramanathan, V. Shanthi, R. Rajasekaran, Identification of potential inhibitors of H5N1 influenza A virus neuraminidase by ligand-based virtual screening approach, Cell Biochem. Biophys. 66 (3) (2013) 657–669.
[50] A. Daina, O. Michielin, V. Zoete, SwissTargetPrediction: updated data and new features for efficient prediction of protein targets of small molecules, Nucleic Acids Res. 47 (W1) (2019) W357–W364.
[51] Sigma-Aldrich H. 1077 Datasheet.
[52] O. Trott, A.J. Olson, AutoDock Vina: improving the speed and accuracy of docking with a new scoring function, efficient optimization, and multithreading, J. Comput. Chem. 31 (2) (2010) 455–461.
[53] F.H. Allen, O. Kennard, D.G. Watson, L. Brammer, A.G. Orpen, R. Taylor, Tables of bond lengths determined by X-ray and neutron diffraction. Part 1. Bond lengths in organic compounds, J. Chem. Soc., Perkin Trans. 2 (12) (1987) S1–S19.
[54] E.E. Langdon-Jones, N.O. Symonds, S.E. Yates, A.J. Hayes, D. Lloyd, R. Williams, S.J. Coles, P.N. Horton, S.J.A. Pope, Fluorescent rhenium-naphthalimide conjugates as cellular imaging agents, Inorg. Chem. 53 (7) (2014) 3788–3797.
[55] X.-Q. Guo, F.N. Castellano, L. Li, H. Szmacinski, J.R. Lakowicz, J. Sipior, A long-lived, highly luminescent Re (I) metal–ligand complex as a biomolecular probe, Anal. Biochem. 254 (2) (1997) 179–186.
[56] J. Axthelm, P. Hoffmann, N. Taye, S. Gläser, H. Görls, S. Hopkins, W. Plass, U. Neugebauer, S. Bonnet, A. Schiller, Co-Registered molecular logic gate with a CO-releasing molecule triggered by light and peroxide, J. Am. Chem. Soc. 139 (14) (2017) 4991–4994.
[57] P. Kumar, R. Kaushik, A. Ghosh, D.A. Jose, Detection of moisture by fluorescent OFF-ON sensor in organic solvents and raw food products, Anal. Chem. 88 (23) (2016) 11314–11318.
[58] J.R. Lakowicz, Principles of Fluorescence Spectroscopy, Springer, US, New York, 2006.
[59] S. Khan, A.M. Malla, A. Zafar, I. Naseem, Synthesis of novel coumarin nucleus-based DPA drug-like molecular entity: In vitro DNA/Cu (II) binding, DNA cleavage and pro-oxidant mechanism for anticancer action, PLoS ONE 12 (8) (2017) e0181783.
[60] R.A. Copeland, J.M. Williams, J. Giannaras, S. Nurnberg, M. Covington, D. Pinto, S. Pick, Trzaskos, Mechanism of selective inhibition of the inducible isoform of prostaglandin G/H synthase, Proc. Natl. Acad. Sci. 91 (23) (1994) 11202–11206.
[61] B. Sunzel, T. Söderberg, C.-O. Reuterving, G. Hallmans, S. Holm, L. Hänström, Neutralizing effect of zinc oxide on dehydroabietic acid-induced toxicity on human polymorphonuclear leukocytes, Biol. Trace Elem. Res. 31 (1) (1991) 33–42.